Editors' Suggestion

Terahertz and High-Harmonic Radiation from Ultrafast Light Subgap or Above-Gap Driving of Spin-Orbit Proximitized Antiferromagnetic Mott Insulator

Federico Garcia-Gaitan,[1] Adrian E. Feiguin,[2] and Branislav K. Nikolić[1,*]
[1]*Department of Physics and Astronomy, University of Delaware, Newark, Delaware 19716, USA*
[2]*Department of Physics, Northeastern University, Boston, Massachusetts 02115, USA*

(Received 21 February 2025; revised 14 July 2025; accepted 16 July 2025; published 22 August 2025; corrected 17 October 2025)

Ultrafast light-driven strongly correlated antiferromagnetic insulators, such as prototypical NiO with a large Mott energy gap ≃4 eV, have recently attracted experimental attention using photons of both subgap [H. Qiu *et al.*, Nat. Phys. **17**, 388 (2021)] and above-gap energy [K. Gillmeister *et al.*, Nat. Commun. **11**, 4095 (2020)]. In the former context, which is also of great interest to applications, emission of terahertz (THz) radiation is observed from NiO/Pt bilayers, where heavy metal (HM) Pt introduces strong spin-orbit coupling (SOC) effects. However, in contrast to amply studied spintronic THz emitters using femtosecond laser pulse (fsLP)-driven FM/HM (where FM represents a ferromagnetic metal of the conventional type, such as Fe, Ni, or Co) bilayers, where ultrafast demagnetization takes place and is directly related to THz emission, microscopic mechanisms of electromagnetic (EM) radiation from NiO/HM bilayers remain obscure, as the total magnetization of NiO is zero before fsLP application. We employ the two-orbital Hubbard-Hund-Heisenberg model and study, via numerically exact quantum many-body methods, the dynamics of its Néel vector and nonequilibrium magnetization. This reveals *nonclassical* (i.e., not describable by the Landau-Lifshitz equation) dynamics of Néel vector and nonequilibrium magnetization, changing only in length while not rotating, where the former is substantially reduced in the case of above-gap fsLPs. Additionally, we compute EM radiation by time dependence of magnetization or of local charge currents, finding that both contributions are significant in the THz frequency range only in NiO with proximity SOC introduced by the HM layer. Outside the THz range, we find an integer high-harmonic generation, as well as unusual noninteger harmonics for the above-gap fsLP pump.

DOI: 10.1103/8dhn-dh55

Introduction—Pump-probe experiments [1] with strongly correlated antiferromagnetic (AFM) insulators (AFIs), such as prototypical NiO [2,3], have revealed [4] exotic effects interweaving nonequilibrium many-body physics and quantum coherence that can persist on surprisingly long timescales (such as ∼1 ps [2,3]) due to a large Mott gap providing protection against fast thermalization and heating after photoexcitation. The femtosecond laser pulse (fsLP) in these experiments and typical theoretical studies [2,3,5] has a central frequency that is above the Mott gap between two Hubbard bands (Fig. 1). In the case of the subgap fsLP pump, theoretical interest has been focused [6–9] on understanding quantum tunneling, multiphoton absorption, and the so-called Keldysh crossover [10,11], as well as the ensuing nonlinear doublon-holon pair production. Such a panoply of complex nonequilibrium many-body states [4] cannot be found in fsLP-driven conventional band insulators and semiconductors governed by single particle quantum effects [12,13].

The same NiO material driven by subgap fsLPs, but in combination with a heavy metal (HM) layer (such as Pt, W, or Ta) introducing effects [19] due to strong spin-orbit coupling (SOC), has very recently been explored [17,18] as a spintronic terahertz (THz) emitter [20–25]. Isolated

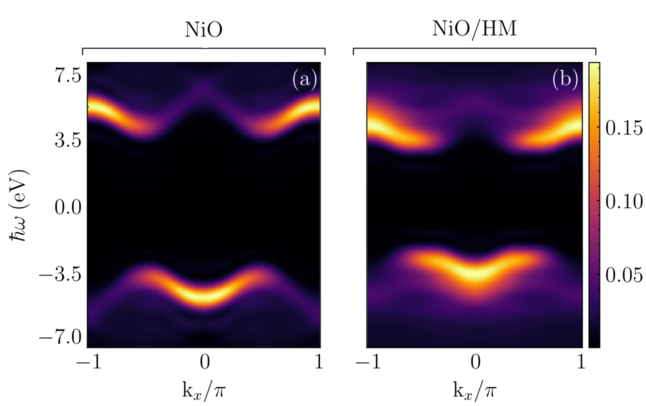

FIG. 1. The tDMRG-computed [14,15] spectral function [16] of the 2HHH model [2] on a ladder (Fig. 2) for (a) plain NiO and (b) NiO with proximity induced Rashba SOC due to an adjacent HM layer within a NiO/HM bilayer employed in THz spintronics experiments [17,18]. The upper and lower Hubbard bands separated by the Mott gap are clearly visible, where we focus on the bonding symmetry sector by choosing $k_y = 0$ [15].

*Contact author: bnikolic@udel.edu

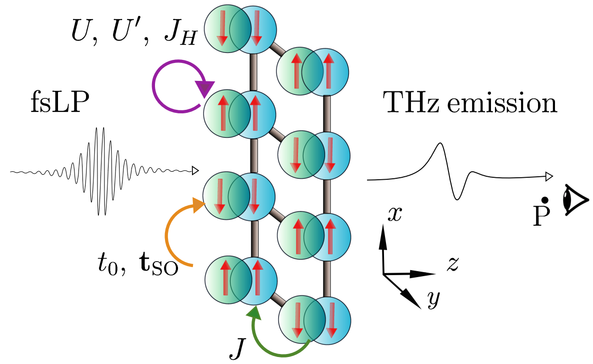

FIG. 2. Schematic view of two-orbitals-per-site 2HHH model [2] for NiO on 4×2 ladder geometry. It can also include additional Rashba SOC [19,46], introduced through $\mathbf{t}_{\mathrm{SO}}$ spin-dependent matrix hoppings [47], as arising from proximity effects [19,48–51] in NiO/HM bilayers employed experimentally [17,18]. Other denoted parameters describing local Coulomb and (U and U') Hund interactions (J_H), Heisenberg exchange interactions (J), and electron hopping (t_0) between sites are explained in Eqs. (2)–(5). This setup is driven out of equilibrium by fsLPs, and we compute EM radiation emitted by it in both the THz and HHG frequency range.

ferromagnetic metal (FM) layers (such as Co, Fe, and Ni) or FM/HM bilayers have been intensely studied for nearly 30 years to understand ultrafast demagnetization [26,27], as well as THz emission by these systems. This emission is much stronger in the case of bilayers [20–24,28] than in the case of a single FM layer [23,28,29]. The fsLP in spintronic experiments typically has a central wavelength of $\simeq$800 nm, so its photons have energy centered around $\hbar\Omega_0 \simeq 1.55$ eV, which is subgap [17,18,30] with respect to the Mott gap $\simeq$4 eV of NiO (Fig. 1). The spintronic phenomena observed in such experiments have been interpreted [17,18] by borrowing the standard intuitive picture [20–24,28,31] (for its recent modifications, however, via microscopic theory, see Refs. [32–34]) developed for FM/HM bilayers. That is, an ultrafast spin current is somehow generated that flows from NiO into the HM layer such that the latter can convert it into charge current via the inverse spin Hall effect [35]. The time-dependent charge current is considered necessary to obtain sizable electromagnetic (EM) radiation in the far-field (FF) region (Fig. 2), as well as to interpret [17,18] the enhancement [23] of the emitted THz radiation when switching from FM to FM/HM systems. This is because magnetic dipole EM radiation [23,28,29] from time-dependent magnetization $\mathbf{M}(t)$ is $1/c$ smaller [32] than EM radiation by a time-dependent charge current, and magnetization of NiO induced out of equilibrium could be minuscule regardless. However, this picture does not explain the microscopic mechanism that generates the assumed spin current in NiO/HM bilayers (there is only speculation thus far [36]), or why the frequency spectrum of such current has features within the 0.1–3 THz range that are imprinted in the EM radiation detected experimentally [17,18]. One can naively expect only that fsLPs will drive electrons into dynamics at its own center frequency Ω_0, as well as at integer (typically odd [37,38]) multiples of Ω_0 for sufficiently intense fsLPs. Such high-harmonic generation (HHG) in current and EM radiation has been vigorously explored lately in diverse quantum materials [39,40], including strongly correlated ones [4,8,9,37,41,42]. Finally, it remains unclear what type of dynamics is obeyed by the Néel vector (as the difference of magnetizations of two sublattices) and magnetization [as the sum of sublattice magnetizations, which is necessarily a nonequilibrium quantity because $\mathbf{M}(t=0) \equiv 0$] when compared to standard demagnetization [23,26,27] of a FM layer whose magnetization vector shrinks. In the case of thin FM layers, a rapid and straightforward analysis of the direction of $\mathbf{M}(t)$ and its magnitude is achieved via magneto-optical Kerr or Faraday effects [23]. In contrast, they do not apply to AFIs, so novel ideas have been explored [43] to detect the presumed rotation of their Néel vector [18,44,45].

Thus, developing a microscopic understanding of the response of AFIs to subgap fsLPs (that is, by starting with a suitable quantum many-body Hamiltonian and using tools of nonequilibrium quantum statistical mechanics) would also help to resolve a number of outstanding issues in AFM optospintronics [52]. Note that, specifically for NiO, which is a strongly correlated material sharing properties of both Mott and charge-transfer insulators [2,3,53], x-ray techniques applied as a probe after a subgap fsLP pump have revealed [30] possible substantial changes of its electronic structure [1,5], such as the emergence of midgap states and Hubbard gap reduction persisting on timescales greater than 2 ps. Such phenomena originating from charge dynamics must be considered together with local spin dynamics, as they can lead to inextricable complex spin-charge dynamics [2,3,54]. In the case of weakly correlated FMs, a proper microscopic description of spin-charge dynamics is achieved via time-dependent density functional theory (TDDFT), which has provided [55–59] a most detailed insight into a sequence of fast-changing events [60] and their effect [31–33] on THz emission. However, applications [61] of TDDFT to NiO are impeded by intricacies including a time-dependent [4,62,63] Hubbard U [64] to properly capture a strong on-site Coulomb interaction that is also dynamical (as opposed to a static U in well-developed conventional equilibrium DFT $+\ U$ calculations [67], where DFT stands for density functional theory).

In this Letter, we aim to capture all the essential physics of strongly correlated electrons within NiO in the presence of fsLPs and SOC by employing a two-orbital Hubbard-Hund-Heisenberg (2HHH) model [2] and by simulating its time evolution via numerically exact quantum many-body methods. Its ground AFM state is formed by local spins $S = 1$ [68] at each site that are composed of two elemental spins $s = 1/2$ located on two orbitals at that site (Fig. 2),

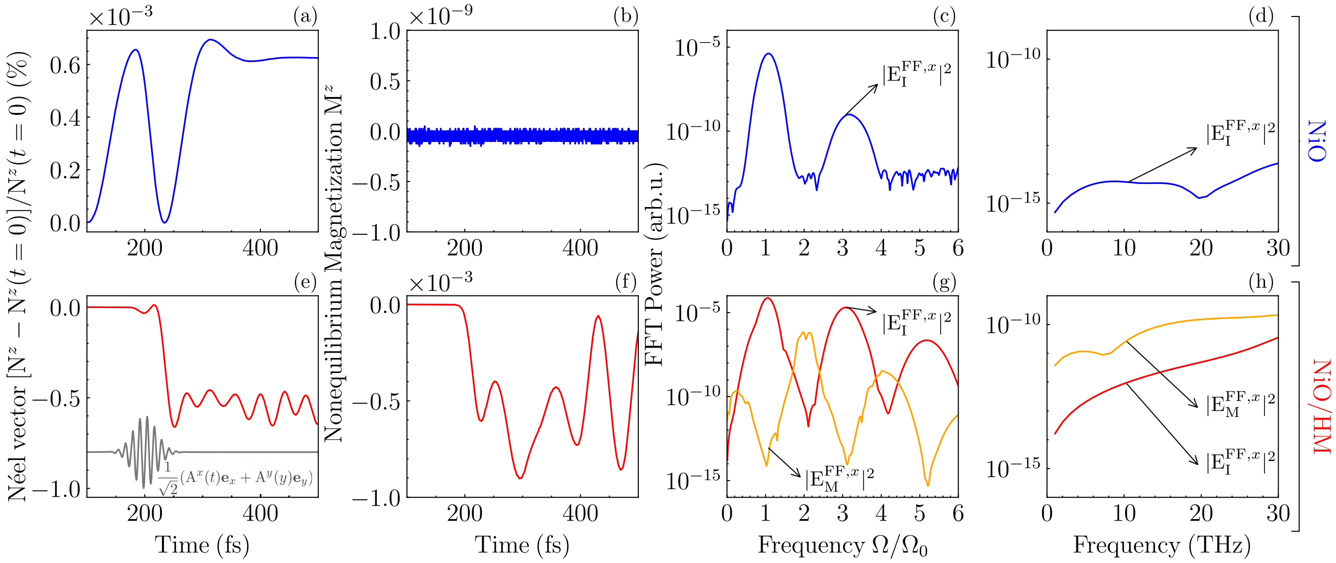

FIG. 3. Time dependence, initiated by a fsLP with subgap central frequency, of (a),(e) the Néel vector and (b),(f) nonequilibrium magnetization. (c),(d),(g),(h) Fast Fourier transform (FFT) power spectrum—within (c),(g) HHG frequencies or (d),(h) THz frequencies—of the x component of the electric field of EM radiation emitted by the dynamics of magnetization [Eq. (A3)] or bond charge currents [Eq. (A2)]. Top row: plain NiO. Bottom row: NiO assumed to contain [19] the Rashba SOC due to proximity effects [48–51] from the HM layer within the NiO/HM bilayer studied in recent experiments [17,18].

with Hund interaction included between them to achieve a fixed and stable S per atom [69,70]. In addition, to consider the adjacent nonmagnetic HM layer in THz spintronics experiments [17,18], we also include SOC of the Rashba type [19,46] in the 2HHH model of Ref. [2]. Thereby introduced SOC models proximity effects [19,48–51] around the NiO/HM interface, which modify the electronic structure on the NiO side due to the HM layer (NiO, in turn, modifies bands of the HM layer, but we do not model the HM layer explicitly due to high computational expense [71]). This model is placed onto a ladder geometry (Fig. 2), allowing for its spectral function (Fig. 1) to be computed [14–16] via numerically (quasi)exact simulations using time-dependent density matrix renormalization group (tDMRG) methods [72–75] applicable to quasi-one-dimensional (quasi-1D) lattices. We complement the study with an additional set of numerical simulations using massively parallel exact diagonalization (ED) methods [76] for Hubbard-type systems, implemented within the HΦ package [77,78]. This technique allows us to access longer times (required for THz radiation calculations) than those possible via tensor network algorithms (like tDMRG) encountering the “entanglement barrier” [79,80]. Our principal results, revealing highly nonclassical dynamics of Néel vector and nonequilibrium magnetization, and the ensuing EM radiation at both HHG of fsLP and in a much lower THz range are given in Figs. 3 and 4. Before discussing these results, we introduce useful concepts and notations.

Model and methods—The monolayer [71] of NiO is modeled on a tight-binding ladder (Fig. 2) with two orbitals per site hosting Ni only, while the O atom is not modeled explicitly, albeit O-mediated interactions are included. The same 2HHH model, but without any SOC, was used in Ref. [2], where above-gap pumping of NiO by fsLP was studied experimentally and theoretically. Our Hamiltonian,

$$\hat{H}_{\rm 2HHH} = \hat{H}_{\rm local} + \hat{H}_{\rm ex} + \hat{H}_{\rm TB} + \hat{H}_{\rm SOC}, \qquad (1)$$

is built on top of the model from Ref. [2] by including proximity induced Rashba SOC [19,46] to describe the NiO/HM bilayer used in THz spintronics experiments [17,18]. The local terms of $\hat{H}_{\rm local}$ account for the Hubbard and Hund physics

$$\begin{aligned}\hat{H}_{\rm local} = {}& U\sum_{i,\alpha}\hat{n}_{i,\alpha\uparrow}\hat{n}_{i,\alpha\downarrow} - \mu\sum_{i,\alpha,\sigma}\hat{n}_{i\alpha\sigma} - g\mu_B B_z^{\rm imp}\hat{s}_{1\alpha}^z \\ & + \sum_{i,\alpha<\beta}\sum_{\sigma,\sigma'}(U' - J_{\rm H}\delta_{\sigma\sigma'})\hat{n}_{i\alpha\sigma}\hat{n}_{i\beta\sigma'} \\ & + \gamma J_{\rm H}\sum_{i,\alpha\neq\beta}(\hat{c}^\dagger_{i\alpha\uparrow}\hat{c}^\dagger_{i\alpha\downarrow}\hat{c}_{i\beta\downarrow}\hat{c}_{i\beta\uparrow} + {\rm H.c.}) \\ & + \gamma J_{\rm H}\sum_{i,\alpha\neq\beta}(\hat{c}^\dagger_{i\alpha\uparrow}\hat{c}^\dagger_{i\beta\downarrow}\hat{c}_{i\alpha\downarrow}\hat{c}_{i\beta\uparrow} + {\rm H.c.}). \end{aligned} \qquad (2)$$

Here $\hat{c}_{i\alpha\sigma}$ ($\hat{c}^\dagger_{i\alpha\sigma}$) is the creation (annihilation) operator of an electron of spin $\sigma = \uparrow, \downarrow$ in orbital $\alpha = 1, 2$ located at site i; $\hat{n}_{i\alpha\sigma}$ is the corresponding number operator; U, U', and $J_{\rm H}$ are the intraorbital Coulomb, interorbital Coulomb, and interorbital (or Hund [69,70]) exchange interaction, respectively; μ is the on-site chemical potential; and $B_z^{\rm imp}$ is a

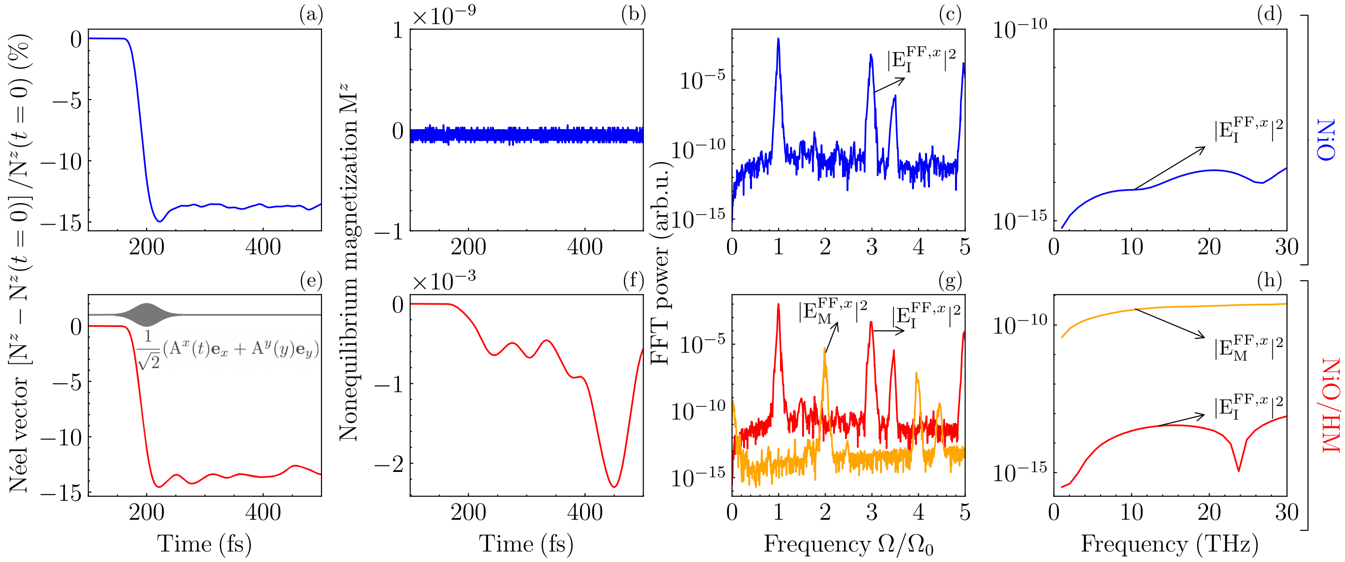

FIG. 4. The same information as in Fig. 3 but using fsLP, whose central frequency of $\hbar\Omega_0 = 8$ eV is above gap in relation to Fig. 1.

magnetic field added [81] on site $i = 1$ to lift the degeneracy between spin-up and spin-down electrons. The Heisenberg exchange interaction between spins at nearest neighbor (NN) sites is given by

$$\hat{H}_{\rm ex} = \sum_{\langle ij\rangle,\alpha} [J(\hat{s}^x_{i\alpha}\cdot\hat{s}^x_{j\alpha} + \hat{s}^y_{i\alpha}\cdot\hat{s}^y_{j\alpha}) + J_z\hat{s}^z_{i\alpha}\cdot\hat{s}^z_{j\alpha}], \quad (3)$$

where $\langle ij\rangle$ denotes summation over the NN sites; $\hat{s}^p_{i\alpha} = \sum_{\sigma,\sigma'}\hat{c}^\dagger_{i\alpha\sigma}\frac{1}{2}\hat{\sigma}^p_{\sigma\sigma'}\hat{c}_{i\alpha\sigma'}$ is the electron spin operator expressed using $\hat{\sigma}^p$ as one of three $(p = x, y, z)$ Pauli matrices; and $J = J_z = 0.1$ eV in the isotropic case. The tight-binding (TB) Hamiltonian

$$\hat{H}_{\rm TB} = -t_0 \sum_{\langle ij\rangle,\alpha,\sigma} (\hat{c}^\dagger_{i\alpha\sigma}\hat{c}_{j\alpha\sigma} + \text{H.c.}), \quad (4)$$

serves as the kinetic term, where t_0 is the hopping parameter. An additional TB term

$$\hat{H}_{\rm SOC} = \sum_{\langle ij\rangle,\alpha} (\hat{\mathbf{c}}^\dagger_{i\alpha}\mathbf{t}_{\rm SO}\hat{\mathbf{c}}_{j\alpha} + \text{H.c.}) \quad (5)$$

is employed to introduce proximity SOC—switched off in the NiO case and switched on in the NiO/HM case in Figs. 3 and 4. Here $\hat{\mathbf{c}}^\dagger_{i\alpha} = (\hat{c}^\dagger_{i\alpha\uparrow}\hat{c}^\dagger_{i\alpha\downarrow})$ denotes the row vector of two creation operators and $\mathbf{t}_{\rm SO}$ is a direction-dependent 2×2 matrix hopping [47] with values $-it_{\rm SO}\hat{\sigma}_y(it_{\rm SO}\hat{\sigma}_x)$ for horizontal (vertical) bonds, where we use $t_{\rm SO} = 0.5$ eV. The $\hat{H}_{\rm SOC}$ term is of the Rashba type [46], assumed to originate from proximity to the HM layer employed experimentally [17,18], as found in conventional equilibrium DFT calculations on FM/HM [19] of AFI/HM [50] bilayers [71]. Realistic parameter values for NiO are taken from prior first-principles calculations for strongly correlated electrons [82], such as from DFT + U [67] and/or DFT plus dynamical mean field theory [83,84] studies: U ≈ 8 eV, $t_0 \approx 1$ eV, and $J_{\rm H} \approx 1$ eV; we set $U' = U - 2J_{\rm H}$ and $\gamma = 1$ for symmetry reasons [85]. Half filling is selected by setting the chemical potential to $\mu = (3U - 5J_H)/2$ [2]. The magnetic field at site 1, $g\mu_B B^{\rm imp}_z = 0.1$ eV, as generated by, e.g., a static impurity, induces [81] Néel "checkerboard" order $\langle\hat{S}^z_i\rangle = -\langle\hat{S}^z_j\rangle \neq 0$ (i and j are two NN sites) in the ground state (GS). Nevertheless, the GS in our simulations retains nonzero entanglement, as witnessed in many recent experiments even at finite temperature [86,87], so it is not identical to an unentangled Néel ket $|\uparrow\downarrow\cdots\uparrow\downarrow\rangle$.

The fsLP is introduced via its vector potential [the gray line in Figs. 3(e) and 4(e)] of amplitude $A_{\rm max}$, which couples to electrons in the form of a Peierls phase [88,89] multiplying hoppings in Eqs. (4) and (5) by a factor $P = \exp[iz_{\rm max}e^{-(t-t_p)^2/2\sigma^2_{\rm light}}\cos(\Omega_0 t)]$, so $t_0(t) = Pt_0$ and $\mathbf{t}_{\rm SO}(t) = P\mathbf{t}_{\rm SO}$ [90]. Here $z_{\rm max} = ea_0A_{\rm max}/\hbar = 0.2$ is the dimensionless parameter [12] quantifying the fsLP intensity, a_0 is the lattice constant, and $\sigma_{\rm light} = 20$ fs determines the width of the Gaussian envelope, which is initially centered at $t_p = 200$ fs. The center frequency of the fsLP is either $\hbar\Omega_0 = 1.55$ eV in Fig. 3, corresponding to a subgap 800 nm wavelength commonly employed in THz spintronic experiments [17,18,20–24,28], or $\hbar\Omega_0 = 8$ eV in Fig. 4 for above-gap fsLP (gaps are shown in Fig. 1). The electric field of the fsLP is linearly polarized along the $x - y$ direction (i.e., diagonal to the ladder) in Fig. 2. The time evolution described by $\hat{H}(t)$ on a 4×2 ladder [92] is computed via massively parallel ED [76] using the HΦ package [77,78], where the GS was found using the Lanczos algorithm and the evolution operator is computed via a Taylor expansion considering up to 15 terms. The time step was chosen as $\delta t = 0.005\hbar/t_0$.

Time-dependent magnetization $M^z(t)$ and Néel vector $N^z(t)$ are obtained by summing spin expectation values at each site, $\mathrm{M}^z = \sum_i M_i^z = \sum_{i,\alpha} \langle \hat{s}^z_{i\alpha} \rangle(t)$ and $\mathrm{N}^z = \sum_i N_i^z \sum_{i,\alpha} (-1)^i \langle \hat{s}^z_{i\alpha} \rangle(t)$, where a "snakelike" enumeration of ladder sites is assumed. Note that other components (the x and y components) are vanishingly small. Our methodology for computing EM radiation, due to time-dependence of bond charge currents I_{ij} or the z-component of nonequilibrium magnetization M^z, is explained in the End Matter.

Results and discussion—The usual first take at interpreting experiments on subgap light-driven AFIs, including NiO [18,101,102], invokes [101–104], a direct coupling of the light magnetic field (or an effective one due to inverse Faraday [102] or inverse Cotton-Mouton [18] effects) to local magnetization of AFIs. This leads to classical dynamics of the Néel vector, which rotates without changing its length [18], in accord with phenomenological theories [44,45] of the Landau-Lifshitz (LL) type [105]. However, limitations of this approach are often found in experiments [102,106], which is not surprising, as light-charge coupling is much stronger [56], so electrons should be explicitly included. But the picture of classical LL dynamics [18,44,45] is appealing because it is difficult to develop intuition on how electrons of AFIs, with a gapped energy spectrum (Fig. 1), absorb subgap light and then affect its magnetic ordering. In the case of AFM metals, it is easy to envisage (and calculate [93]) that fsLP generates a photocurrent of conduction electrons, which are then spin polarized by the magnetic background and exert spin torque [93] onto local magnetization. Its dynamics follow (for weak-intensity fsLP to avoid demagnetization [26,27]) classical LL dynamics. Note that such dynamics can be justified only for AFs whose localized spins are $S > 1$ and for sufficiently high temperatures of their dissipative environment [107].

For AFIs, where the Hubbard interaction is much stronger than in the metallic case, there is no such shortcut, and one has to handle the complexities of the photoexcited Hubbard model [4–9,108]. In addition, because NiO hosts localized spins $S = 1$, we can anticipate [107] their nonclassical (i.e., outside of any description by LL-type theories [18,44]) dynamics. Indeed, our quantum many-body calculations for subgap fsLP-driven NiO reveal highly nonclassical [81,109,110] dynamics of the Néel vector and magnetization in Fig. 3. That is, both vectors are changing length along the z axis (orthogonal to the ladder in Fig. 2) while not rotating at all. Nonequilibrium magnetization remains zero in plain NiO [Fig. 3(b)]. However, $M^z(t) \neq 0$ in SO proximitized NiO [Fig. 3(f)], which is akin to experimentally observed [111] weak ferromagnetism in a photodoped Mott insulator with native SOC. The nonzero $\partial_t^2 M^z(t_r)$ emits magnetic dipole [Eq. (A3)] THz radiation [the orange line in Fig. 3(h)], which can (surprisingly, when compared to FM/HM bilayers [32]) surpass the contribution from $\partial_t I_{ij}(t_r)$ [the red curve in Fig. 3(h)]. Importantly, THz emission from both of these two sources is significant only when proximity SOC is present in NiO/HM bilayer [Fig. 3(h)], in full accord with experiments [17,18]. Thus, our theory explains these experiments without invoking qualitative speculations [17,18,36], while showing that concepts borrowed from FM/HM systems (like interlayer spin current and spin-to-charge conversion within HMs [20,21,23,24,28,33]) are not necessary for THz emission from an AFI. The magnetic dipole EM radiation exhibits even integer HHG [Fig. 3(g)], while odd ones are expected [37] for radiation from $\partial_t I_{ij}(t_r)$, as dictated by symmetry-imposed selection rules of Floquet group theory [112]. Although SOC breaks inversion symmetry, odd integer HHG is preserved [38,113]. This offers a scheme—detect even HHG in EM radiation from an AFI—which directly corroborates how magnetization dynamics in magnets driven by fsLP can be much faster [58,114] than observed in low-energy transport experiments [36].

For above-gap fsLP in Fig. 4, we find reduction of Néel vector by up to 15%, signifying suppression [5] of AFM order in the GS. This is in sharp contrast to its minuscule change for subgap fsLP in Fig. 3. As with subgap fsLPs, nonequilibrium magnetization [compare Figs. 4(f) and 4(b)] emerges only when proximity SOC in switched on. Unlike the subgap fsLP case, the charge current and its THz radiation are not significantly enhanced by including proximity SOC [Fig. 4(d) vs Fig. 4(h)]. The selection rules for HHG remain the same, allowing only odd integer HHG of $E_I^{\mathrm{FF},x}$ [Figs. 4(c) and 4(g)] and even ones of $E_M^{\mathrm{FF},x}$ [Fig. 4(g)]. Curiously, we also find noninteger HHG [Figs. 4(c) and 4(g)] of both $E_I^{\mathrm{FF},x}$ and $E_M^{\mathrm{FF},x}$, which are beyond standard Floquet theory and its selection rules [112]. Theoretical [37,96] and experimental reports [40] of noninteger HHG are scarce [4], and their understanding is in its infancy. For example, they could arise [37] from a correlation-driven population of multiple Floquet states (unlike the population of a single state used in Floquet group theory [112]), whose exploration we relegate to future studies [115].

Acknowledgments—F. G-G. and B. K. N. were supported by the U.S. National Science Foundation (NSF) through the University of Delaware Materials Research Science and Engineering Center (NSF Award No. DMR-2011824). The supercomputing time was provided by the Delaware Advanced Research Workforce and Innovation Network (DARWIN), which is supported by NSF Award No. MRI-1919839. A. E. F. was supported by the U.S. Department of Energy, Office of Basic Energy Sciences, under Award No. DE-SC0022311.

Data availability—The data that support the findings of this Letter are not publicly available upon publication because it is not technically feasible and/or the cost of preparing, depositing, and hosting the data would be prohibitive within the terms of this research project. The data are available from the authors upon reasonable request.

[1] Y. Wang, M. Claassen, C. D. Pemmaraju, C. Jia, B. Moritz, and T. P. Devereaux, Theoretical understanding of photon spectroscopies in correlated materials in and out of equilibrium, Nat. Rev. Mater. **3**, 312 (2018).

[2] K. Gillmeister, D. Golež, C.-T. Chiang, N. Bittner, Y. Pavlyukh, J. Berakdar, P. Werner, and W. Widdra, Ultrafast coupled charge and spin dynamics in strongly correlated NiO, Nat. Commun. **11**, 4095 (2020).

[3] G. Merzoni, L. Martinelli, S. Parchenko, S. F. R. TenHuisen, V. Lebedev, L. Adriano, R. Carley, N. Gerasimova, L. Mercadier, M. Teichmann *et al.*, Photogenerated charge-transfer excitons in NiO revealed by ultrafast time-resolved resonant inelastic x-ray scattering, arXiv:2504.16653.

[4] Y. Murakami, D. Golež, M. Eckstein, and P. Werner, Photo-induced nonequilibrium states in Mott insulators, Rev. Mod. Phys. **97**, 035001 (2025).

[5] Y. Wang, M. Claassen, B. Moritz, and T. P. Devereaux, Producing coherent excitations in pumped Mott antiferromagnetic insulators, Phys. Rev. B **96**, 235142 (2017).

[6] T. Oka, Nonlinear doublon production in a Mott insulator: Landau-Dykhne method applied to an integrable model, Phys. Rev. B **86**, 075148 (2012).

[7] K. Shinjo, S. Sota, and T. Tohyama, Glassy dynamics of the one-dimensional Mott insulator excited by a strong terahertz pulse, Phys. Rev. Res. **4**, L032019 (2022).

[8] Y. Murakami, M. Eckstein, and P. Werner, High-harmonic generation in Mott insulators, Phys. Rev. Lett. **121**, 057405 (2018).

[9] Y. Murakami, S. Takayoshi, A. Koga, and P. Werner, High-harmonic generation in one-dimensional Mott insulators, Phys. Rev. B **103**, 035110 (2021).

[10] K. Shinjo and T. Tohyama, Keldysh crossover in one-dimensional Mott insulators, APL Mater. **12**, 041109 (2024).

[11] R. Andrei, M. Guo, M. Ali, H. Kim, R. D. Averitt, D. Hsieh, and E. Demler, Subgap pumping of antiferromagnetic Mott insulators: Photoexcitation mechanisms and applications, arXiv:2505.15343.

[12] U. Bajpai, B. S. Popescu, P. Plecháč, B. K. Nikolić, L. E. F. Foa Torres, H. Ishizuka, and N. Nagaosa, Spatio-temporal dynamics of shift current quantum pumping by femtosecond light pulse, J. Phys. Mater. **2**, 025004 (2019).

[13] K. Yonemitsu, Photoinduced dynamics and nonequilibrium characteristics in quasi-one-dimensional effectron systems: Mott insulators vs band insulators, J. Phys. Conf. Ser. **21**, 30 (2005).

[14] K. Zawadzki and A. E. Feiguin, Time- and momentum-resolved tunneling spectroscopy of pump-driven nonthermal excitations in Mott insulators, Phys. Rev. B **100**, 195124 (2019).

[15] C. Yang and A. E. Feiguin, Spectral function of Mott-insulating Hubbard ladders: From fractionalized excitations to coherent quasiparticles, Phys. Rev. B **99**, 235117 (2019).

[16] G. W. Winkler, M. Ganahl, D. Schuricht, H. G. Evertz, and S. Andergassen, Interaction effects in a microscopic quantum wire model with strong spin–orbit interaction, New J. Phys. **19**, 063009 (2017).

[17] H. Qiu, L. Zhou, C. Zhang, J. Wu, Y. Tian, S. Cheng, S. Mi, H. Zhao, Q. Zhang, D. Wu *et al.*, Ultrafast spin current generated from an antiferromagnet, Nat. Phys. **17**, 388 (2021).

[18] E. Rongione, O. Gueckstock, M. Mattern, O. Gomonay, H. Meer, C. Schmitt, R. Ramos, T. Kikkawa, M. Mičica, E. Saitoh *et al.*, Emission of coherent THz magnons in an antiferromagnetic insulator triggered by ultrafast spin-phonon interactions, Nat. Commun. **14**, 1818 (2023).

[19] S. Grytsyuk, A. Belabbes, P. M. Haney, H.-W. Lee, K.-J. Lee, M. D. Stiles, U. Schwingenschlögl, and A. Manchon, k-asymmetric spin splitting at the interface between transition metal ferromagnets and heavy metals, Phys. Rev. B **93**, 174421 (2016).

[20] T. Seifert, S. Jaiswal, U. Martens, J. Hannegan, L. Braun, P. Maldonado, F. Freimuth, A. Kronenberg, J. Henrizi, I. Radu *et al.*, Efficient metallic spintronic emitters of ultrabroadband terahertz radiation, Nat. Photonics **10**, 483 (2016).

[21] Y. Wu, M. Elyasi, X. Qiu, M. Chen, Y. Liu, L. Ke, and H. Yang, High-performance THz emitters based on ferromagnetic/nonmagnetic heterostructures, Adv. Mater. **29**, 1603031 (2017).

[22] M. B. Jungfleisch, Q. Zhang, W. Zhang, J. E. Pearson, R. D. Schaller, H. Wen, and A. Hoffmann, Control of terahertz emission by ultrafast spin-charge current conversion at Rashba interfaces, Phys. Rev. Lett. **120**, 207207 (2018).

[23] R. Rouzegar, L. Brandt, L. Nádvorník, D. A. Reiss, A. L. Chekhov, O. Gueckstock, C. In, M. Wolf, T. S. Seifert, P. W. Brouwer, G. Woltersdorf, and T. Kampfrath, Laser-induced terahertz spin transport in magnetic nanostructures arises from the same force as ultrafast demagnetization, Phys. Rev. B **106**, 144427 (2022).

[24] T. S. Seifert, D. Go, H. Hayashi, R. Rouzegar, F. Freimuth, K. Ando, Y. Mokrousov, and T. Kampfrath, Time-domain observation of ballistic orbital-angular-momentum currents with giant relaxation length in tungsten, Nat. Nanotechnol. **18**, 1132 (2023).

[25] A. Leitenstorfer, A. S. Moskalenko, T. Kampfrath, J. Kono, E. Castro-Camus, K. Peng, N. Qureshi, D. Turchinovich, K. Tanaka, A. G. Markelz *et al.*, The 2023 terahertz science and technology roadmap, J. Phys. D **56**, 223001 (2023).

[26] E. Beaurepaire, J.-C. Merle, A. Daunois, and J.-Y. Bigot, Ultrafast spin dynamics in ferromagnetic nickel, Phys. Rev. Lett. **76**, 4250 (1996).

[27] X. Chen, R. Adam, D. E. Bürgler, F. Wang, Z. Lu, L. Pan, S. Heidtfeld, C. Greb, M. Liu, Q. Liu, J. Wang, C. M. Schneider, and D. Cao, Ultrafast demagnetization in ferromagnetic materials: Origins and progress, Phys. Rep. **1102**, 1 (2025).

[28] Y. Liu, H. Cheng, Y. Xu, P. Vallobra, S. Eimer, X. Zhang, X. Wu, T. Nie, and W. Zhao, Separation of emission

mechanisms in spintronic terahertz emitters, Phys. Rev. B **104**, 064419 (2021).

[29] E. Beaurepaire, G. M. Turner, S. M. Harrel, M. C. Beard, J.-Y. Bigot, and C. A. Schmuttenmaer, Coherent terahertz emission from ferromagnetic films excited by femtosecond laser pulses, Appl. Phys. Lett. **84**, 3465 (2004).

[30] X. Wang, R. Y. Engel, I. Vaskivskyi, D. Turenne, V. Shokeen, A. Yaroslavtsev, O. Grånäs, R. Knut, J. O. Schunck, S. Dziarzhytski *et al.*, Ultrafast manipulation of the NiO antiferromagnetic order via sub-gap optical excitation, Faraday Discuss. **237**, 300 (2022).

[31] F. Foggetti and P. M. Oppeneer, Quantitative modeling of spintronic terahertz emission due to ultrafast spin transport, Phys. Rev. Appl. **23**, 014067 (2025).

[32] A. Kefayati and B. K. Nikolić, Origins of electromagnetic radiation from spintronic terahertz emitters: A time-dependent density functional theory plus Jefimenko equations approach, Phys. Rev. Lett. **133**, 136704 (2024).

[33] A. Kefayati, Y. Ren, M. B. Jungfleisch, L. Gundlach, J. Q. Xiao, and B. K. Nikolić, Deciphering the origin of spin current in spintronic terahertz emitters and its imprint on their electromagnetic radiation via time-dependent density functional theory, Phys. Rev. B **111**, L140415 (2025).

[34] J. Varela-Manjarres, A. Kefayati, M. B. Jungfleisch, J. Q. Xiao, and B. K. Nikolić, Charge and spin current pumping by ultrafast demagnetization dynamics, Phys. Rev. B **110**, L060410 (2024).

[35] E. Saitoh, M. Ueda, H. Miyajima, and G. Tatara, Conversion of spin current into charge current at room temperature: Inverse spin-Hall effect, Appl. Phys. Lett. **88**, 182509 (2006).

[36] J. Han, R. Cheng, L. Liu, H. Ohno, and S. Fukami, Coherent antiferromagnetic spintronics, Nat. Mater. **22**, 684 (2023).

[37] C. S. Lange, T. Hansen, and L. B. Madsen, Noninteger high-order harmonic generation from extended correlated systems, Phys. Rev. A **109**, 063103 (2024).

[38] N. Tancogne-Dejean, F. G. Eich, and A. Rubio, Effect of spin-orbit coupling on the high harmonics from the topological Dirac semimetal Na_3Bi, npj Comput. Mater. **8**, 145 (2022).

[39] S. Ghimire and D. A. Reis, High-harmonic generation from solids, Nat. Phys. **15**, 10 (2018).

[40] C. P. Schmid, L. Weigl, P. Grössing, V. Junk, C. Gorini, S. Schlauderer, S. Ito, M. Meierhofer, N. Hofmann, D. Afanasiev *et al.*, Tunable non-integer high-harmonic generation in a topological insulator, Nature (London) **593**, 385 (2021).

[41] S. Imai, A. Ono, and S. Ishihara, High harmonic generation in a correlated electron system, Phys. Rev. Lett. **124**, 157404 (2020).

[42] C. Orthodoxou, A. Zaïr, and G. H. Booth, High harmonic generation in two-dimensional Mott insulators, npj Quantum Mater. **6**, 76 (2021).

[43] V. Saidl, P. Němec, P. Wadley, V. Hills, R. P. Campion, V. Novák, K. W. Edmonds, F. Maccherozzi, S. S. Dhesi, B. L. Gallagher *et al.*, Optical determination of the Néel vector in a CuMnAs thin-film antiferromagnet, Nat. Photonics **11**, 91 (2017).

[44] E. G. Galkina and B. A. Ivanov, Phenomenological description of spin dynamics in antiferromagnets: Short history and modern development, Low Temp. Phys. **47**, 765 (2021).

[45] H. V. Gomonay and V. M. Loktev, Spin transfer and current-induced switching in antiferromagnets, Phys. Rev. B **81**, 144427 (2010).

[46] A. Manchon, H. C. Koo, J. Nitta, S. M. Frolov, and R. A. Duine, New perspectives for Rashba spin-orbit coupling, Nat. Mater. **14**, 871 (2015).

[47] B. K. Nikolić, L. P. Zârbo, and S. Souma, Imaging mesoscopic spin Hall flow: Spatial distribution of local spin currents and spin densities in and out of multiterminal spin-orbit coupled semiconductor nanostructures, Phys. Rev. B **73**, 075303 (2006).

[48] J. M. Marmolejo-Tejada, K. Dolui, P. Lazić, P.-H. Chang, S. Smidstrup, D. Stradi, K. Stokbro, and B. K. Nikolić, Proximity band structure and spin textures on both sides of topological-insulator/ferromagnetic-metal interface and their charge transport probes, Nano Lett. **17**, 5626 (2017).

[49] K. Dolui, U. Bajpai, and B. K. Nikolić, Effective spin-mixing conductance of topological-insulator/ferromagnet and heavy-metal/ferromagnet spin-orbit-coupled interfaces: A first-principles Floquet-nonequilibrium Green function approach, Phys. Rev. Mater. **4**, 121201(E) (2020).

[50] K. Dolui, A. Suresh, and B. K. Nikolić, Spin pumping from antiferromagnetic insulator spin-orbit-proximitized by adjacent heavy metal: A first-principles Floquet-nonequilibrium Green function study, J. Nonlinear Opt. Phys. Mater. **5**, 034002 (2022).

[51] I. Žutić, A. Matos-Abiague, B. Scharf, H. Dery, and K. Belashchenko, Proximitized materials, Mater. Today **22**, 85 (2019).

[52] P. Němec, M. Fiebig, T. Kampfrath, and A. V. Kimel, Antiferromagnetic opto-spintronics, Nat. Phys. **14**, 229 (2018).

[53] F. Lechermann, W. Körner, D. F. Urban, and C. Elsässer, Interplay of charge-transfer and Mott-Hubbard physics approached by an efficient combination of self-interaction correction and dynamical mean-field theory, Phys. Rev. B **100**, 115125 (2019).

[54] N. Bittner, D. Golež, H. U. R. Strand, M. Eckstein, and P. Werner, Coupled charge and spin dynamics in a photo-excited doped Mott insulator, Phys. Rev. B **97**, 235125 (2018).

[55] K. Krieger, J. K. Dewhurst, P. Elliott, S. Sharma, and E. K. U. Gross, Laser-induced demagnetization at ultrashort time scales: Predictions of TDDFT, J. Chem. Theory Comput. **11**, 4870 (2015).

[56] Z. Chen and L.-W. Wang, Role of initial magnetic disorder: A time-dependent ab initio study of ultrafast demagnetization mechanisms, Sci. Adv. **5**, eaau8000 (2019).

[57] N. Wu, S. Zhang, D. Chen, Y. Wang, and S. Meng, Three-stage ultrafast demagnetization dynamics in a monolayer ferromagnet, Nat. Commun. **15**, 2804 (2024).

[58] M. S. Mrudul and P. M. Oppeneer, *Ab initio* investigation of laser-induced ultrafast demagnetization of $L1_0$ FePt: Intensity dependence and importance of electron coherence, Phys. Rev. B **109**, 144418 (2024).

[59] V. Shokeen, M. Sanchez Piaia, J.-Y. Bigot, T. Müller, P. Elliott, J. K. Dewhurst, S. Sharma, and E. K. U. Gross, Spin flips versus spin transport in nonthermal electrons excited by ultrashort optical pulses in transition metals, Phys. Rev. Lett. **119**, 107203 (2017).

[60] P. Tengdin, W. You, C. Chen, X. Shi, D. Zusin, Y. Zhang, C. Gentry, A. Blonsky, M. Keller, P. M. Oppeneer *et al.*, Critical behavior within 20 fs drives the out-of-equilibrium laser-induced magnetic phase transition in nickel, Sci. Adv. **4**, eaap9744 (2018).

[61] J. K. Dewhurst, P. Elliott, S. Shallcross, E. K. U. Gross, and S. Sharma, Laser-induced intersite spin transfer, Nano Lett. **18**, 1842 (2018).

[62] N. Tancogne-Dejean, M. A. Sentef, and A. Rubio, Ultrafast modification of Hubbard U in a strongly correlated material: *Ab initio* high-harmonic generation in NiO, Phys. Rev. Lett. **121**, 097402 (2018).

[63] O. K. Orhan and D. D. O'Regan, TDDFT $+ U$: A critical assessment of the Hubbard U correction to exchange-correlation kernels and potentials, Phys. Rev. B **99**, 165120 (2019).

[64] Note that TDDFT studies [65,66] of even standard $3d$ transition metal ferromagnets—such as Fe, Co, and Ni—have recently started to explore additional effects on ultrafast demagnetization due to Coulomb correlations among the localized d electrons included via the Hubbard U.

[65] S. R. Acharya, V. Turkowski, G. P. Zhang, and T. S. Rahman, Ultrafast electron correlations and memory effects at work: Femtosecond demagnetization in Ni, Phys. Rev. Lett. **125**, 017202 (2020).

[66] T. Barros, N. Tancogne-Dejean, J. Berakdar, and M. A. L. Marques, Impact of electron correlation on the light-induced demagnetization of elemental ferromagnetic metals, Eur. Phys. J. B **95**, 175 (2022).

[67] V. I. Anisimov, J. Zaanen, and O. K. Andersen, Band theory and Mott insulators: Hubbard U instead of Stoner I, Phys. Rev. B **44**, 943 (1991).

[68] A. Nag, H. C. Robarts, F. Wenzel, J. Li, H. Elnaggar, R.-P. Wang, A. C. Walters, M. García-Fernández, F. M. F. de Groot, M. W. Haverkort *et al.*, Many-body physics of single and double spin-flip excitations in NiO, Phys. Rev. Lett. **124**, 067202 (2020).

[69] M. Hoffmann and S. Blügel, Systematic derivation of realistic spin models for beyond-Heisenberg solids, Phys. Rev. B **101**, 024418 (2020).

[70] K. M. Stadler, G. Kotliar, S.-S. B. Lee, A. Weichselbaum, and J. von Delft, Differentiating Hund from Mott physics in a three-band Hubbard-Hund model: Temperature dependence of spectral, transport, and thermodynamic properties, Phys. Rev. B **104**, 115107 (2021).

[71] Note that despite the complex band structure on both sides [48,50] (i.e., due to the two materials affecting each other via proximity effects [51]) of FM/HM or AFI/HM heterostructures, the odd-in-**k**-vector spin splitting of interfacial bands often found in DFT calculations [19,48] displays remarkable similarities [19] to the much simpler Rashba SOC model [Eq. (5)]. Although overlap of interfacial orbitals plays an important role in DFT calculations—generating effects [19] like correlation between the spin-splitting strength of the bands and the SOC-weighted induced orbital momentum, as well as orbital charge transfer—we do not model it explicitly by adding a second NM layer with its own orbitals (aside from two selected orbitals per site of NiO layer in Fig. 2 that we model explicitly) due to high computational expense of our quantum many-body calculations (when compared to effective single-body calculations of DFT). Nevertheless, the essential outcome of such complex interfacial processes is included in our Hamiltonian through the Rashba SOC term [Eq. (5)], i.e., as **k**-asymmetric spin splitting [Fig. 1(b)]. Most importantly, our finding that THz emission is significant only when the Rashba SOC is turned on, as well as that in experiments the highest intensity of THz radiation comes from the thinnest NiO layer, is fully compatible with findings of recent experiments [17,18] on subgap-fsLP-excited NiO/HM bilayers.

[72] S. R. White and A. E. Feiguin, Real-time evolution using the density matrix renormalization group, Phys. Rev. Lett. **93**, 076401 (2004).

[73] A. J. Daley, C. Kollath, U. Schollwöck, and G. Vidal, Time-dependent density-matrix renormalization-group using adaptive effective Hilbert spaces, J. Stat. Mech. (2004) P04005.

[74] P. Schmitteckert, Nonequilibrium electron transport using the density matrix renormalization group method, Phys. Rev. B **70**, 121302(R) (2004).

[75] A. E. Feiguin, The density matrix renormalization group and its time-dependent variants, AIP Conf. Proc. **1419**, 5 (2011).

[76] M. Innerberger, P. Worm, P. Prauhart, and A. Kauch, Electron-light interaction in nonequilibrium: Exact diagonalization for time-dependent Hubbard Hamiltonians, Eur. Phys. J. Plus **135**, 922 (2020).

[77] K. Ido, M. Kawamura, Y. Motoyama, K. Yoshimi, Y. Yamaji, S. Todo, N. Kawashima, and T. Misawa, Update of HΦ: Newly added functions and methods in versions 2 and 3, Comput. Phys. Commun. **298**, 109093 (2024).

[78] M. Kawamura, K. Yoshimi, T. Misawa, Y. Yamaji, S. Todo, and N. Kawashima, Quantum lattice model solver HΦ, Comput. Phys. Commun. **217**, 180 (2017).

[79] M. M. Rams and M. Zwolak, Breaking the entanglement barrier: Tensor network simulation of quantum transport, Phys. Rev. Lett. **124**, 137701 (2020).

[80] A. Lerose, M. Sonner, and D. A. Abanin, Overcoming the entanglement barrier in quantum many-body dynamics via space-time duality, Phys. Rev. B **107**, L060305 (2023).

[81] M. D. Petrović, P. Mondal, A. E. Feiguin, and B. K. Nikolić, Quantum spin torque driven transmutation of an antiferromagnetic Mott insulator, Phys. Rev. Lett. **126**, 197202 (2021).

[82] K. Held, Electronic structure calculations using dynamical mean field theory, Adv. Phys. **56**, 829 (2007).

[83] J. Kuneš, V. I. Anisimov, A. V. Lukoyanov, and D. Vollhardt, Local correlations and hole doping in NiO: A dynamical mean-field study, Phys. Rev. B **75**, 165115 (2007).

[84] L. Zhang, P. Staar, A. Kozhevnikov, Y.-P. Wang, J. Trinastic, T. Schulthess, and H.-P. Cheng, DFT $+$ DMFT calculations

of the complex band and tunneling behavior for the transition metal monoxides MnO, FeO, CoO, and NiO, Phys. Rev. B **100**, 035104 (2019).

[85] J. Rincón, E. Dagotto, and A. E. Feiguin, Photoinduced Hund excitons in the breakdown of a two-orbital Mott insulator, Phys. Rev. B **97**, 235104 (2018).

[86] A. Scheie, P. Laurell, A. M. Samarakoon, B. Lake, S. E. Nagler, G. E. Granroth, S. Okamoto, G. Alvarez, and D. A. Tennant, Witnessing entanglement in quantum magnets using neutron scattering, Phys. Rev. B **103**, 224434(2021).

[87] P. Laurell, A. Scheie, E. Dagotto, and D. A. Tennant, Witnessing entanglement and quantum correlations in condensed matter: A review, Adv. Quantum Technol. **8**, 2400196 (2025).

[88] G. Panati, H. Spohn, and S. Teufel, Effective dynamics for Bloch electrons: Peierls substitution and beyond, Commun. Math. Phys. **242**, 547 (2003).

[89] J. Li, D. Golez, G. Mazza, A. J. Millis, A. Georges, and M. Eckstein, Electromagnetic coupling in tight-binding models for strongly correlated light and matter, Phys. Rev. B **101**, 205140 (2020).

[90] We have verified that our results are largely insensitive to the inclusion of additional terms required for multiorbital systems [4,91], such as $\mathbf{E}(t)\cdot\mathbf{P}(t)$, where $\mathbf{E}(t) = -\partial_t\mathbf{A}$ is the electric field of fsLP and $\mathbf{P}(t)$ describes the dipolar matrix elements between different orbitals residing on the same site of the lattice.

[91] Y. Murakami, M. Schüler, S. Takayoshi, and P. Werner, Ultrafast nonequilibrium evolution of excitonic modes in semiconductors, Phys. Rev. B **101**, 035203 (2020).

[92] This is the largest lattice size, hosting two orbitals per site, that we could simulate within a reasonable computational time. For example, the storage cost of the sparse Hamiltonian matrix alone defined for this lattice exceeds 600 GB. Nevertheless, using such a small ladder is already sufficient to capture various dissipative mechanisms, even in the absence of phonons that are considered necessary for relaxation [57,93] after weakly correlated magnets are excited by fsLP. For example, in quasi-1D ladder geometry [94,95], and with more than one orbital per site [85], spin-charge separation characterizing 1D Mott insulators [96,97] is suppressed. This opens [85,94] dissipation channels due to electron-spin interaction, where energy is transferred from the electrons to the AFM background [2,4,95], as well as local dissipation caused by the Hund interaction [85,98,99]. The outcome is that photoexcited charge current decays, even though phonons are absent, as shown in the Supplemental Material [100].

[93] A. Suresh and B. K. Nikolić, Quantum classical approach to spin and charge pumping and the ensuing radiation in terahertz spintronics: Example of the ultrafast light-driven Weyl antiferromagnet Mn_3Sn, Phys. Rev. B **107**, 174421 (2023).

[94] M. Eckstein and P. Werner, Ultra-fast photo-carrier relaxation in Mott insulators with short-range spin correlations, Sci. Rep. **6**, 21235 (2016).

[95] D. Golež, J. Bonča, M. Mierzejewski, and L. Vidmar, Mechanism of ultrafast relaxation of a photo-carrier in antiferromagnetic spin background, Phys. Rev. B **89**, 165118 (2014).

[96] Y. Murakami, T. Hansen, S. Takayoshi, L. B. Madsen, and P. Werner, Many-body effects on high-harmonic generation in Hubbard ladders, Phys. Rev. Lett. **134**, 096504 (2025).

[97] Y. Murakami, S. Takayoshi, T. Kaneko, A. M. Läuchli, and P. Werner, Spin, charge, and η-spin separation in one-dimensional photodoped Mott insulators, Phys. Rev. Lett. **130**, 106501 (2023).

[98] M. Lysne, Y. Murakami, and P. Werner, Signatures of bosonic excitations in high-harmonic spectra of Mott insulators, Phys. Rev. B **101**, 195139 (2020).

[99] H. U. R. Strand, D. Golež, M. Eckstein, and P. Werner, Hund's coupling driven photocarrier relaxation in the two-band Mott insulator, Phys. Rev. B **96**, 165104 (2017).

[100] See Supplemental Material at http://link.aps.org/supplemental/10.1103/8dhn-dh55 for an additional figure showing how the sum of all bond charge currents decays with increasing on-site Coulomb interaction due to thereby enabled dissipation of electron energy into bosonic excitations of AFM ordered background [2,94,95].

[101] T. Kampfrath, A. Sell, G. Klatt, A. Pashkin, S. Mährlein, T. Dekorsy, M. Wolf, M. Fiebig, A. Leitenstorfer, and R. Huber, Coherent terahertz control of antiferromagnetic spin waves, Nat. Photonics **5**, 31 (2011).

[102] T. Satoh, S.-J. Cho, R. Iida, T. Shimura, K. Kuroda, H. Ueda, Y. Ueda, B. A. Ivanov, F. Nori, and M. Fiebig, Spin oscillations in antiferromagnetic NiO triggered by circularly polarized light, Phys. Rev. Lett. **105**, 077402 (2010).

[103] A. V. Kimel, B. A. Ivanov, R. V. Pisarev, P. A. Usachev, A. Kirilyuk, and T. Rasing, Inertia-driven spin switching in antiferromagnets, Nat. Phys. **5**, 727 (2009).

[104] T. G. H. Blank, K. A. Grishunin, B. A. Ivanov, E. A. Mashkovich, D. Afanasiev, and A. V. Kimel, Empowering control of antiferromagnets by THz-induced spin coherence, Phys. Rev. Lett. **131**, 096701 (2023).

[105] L. D. Landau and E. M. Lifshitz, On the theory of the dispersion of magnetic permeability in ferromagnetic bodies, Phys. Z. Sowjetunion **8**, 153 (1935).

[106] F. Formisano, T. T. Gareev, D. I. Khusyainov, A. E. Fedianin, R. M. Dubrovin, P. P. Syrnikov, D. Afanasiev, R. V. Pisarev, A. M. Kalashnikova, J. H. Mentink *et al.*, Coherent THz spin dynamics in antiferromagnets beyond the approximation of the Néel vector, APL Mater. **12**, 011105 (2024).

[107] F. Garcia-Gaitan and B. K. Nikolić, Fate of entanglement in magnetism under Lindbladian or non-Markovian dynamics and conditions for their transition to Landau-Lifshitz-Gilbert classical dynamics, Phys. Rev. B **109**, L180408 (2024).

[108] J. H. Mentink, K. Balzer, and M. Eckstein, Ultrafast and reversible control of the exchange interaction in Mott insulators, Nat. Commun. **6**, 6708 (2015).

[109] A. Mitrofanov and S. Urazhdin, Nonclassical spin transfer effects in an antiferromagnet, Phys. Rev. Lett. **126**, 037203 (2021).

[110] T. Lee, M. T. Park, H.-W. Ko, J. H. Oh, S. Ko, S. Hwang, J. G. Jang, G.-W. Baek, S. K. Kim, H.-W. Lee, M.-H. Jung, K.-J. Kim, and K.-J. Lee, Signatures of longitudinal spin

pumping in a magnetic phase transition, Nature (London) **638**, 106 (2025).
[111] D. Afanasiev, A. Gatilova, D. J. Groenendijk, B. A. Ivanov, M. Gibert, S. Gariglio, J. Mentink, J. Li, N. Dasari, M. Eckstein *et al.*, Ultrafast spin dynamics in photodoped spin-orbit Mott insulator Sr_2IrO_4, Phys. Rev. X **9**, 021020 (2019).
[112] O. Neufeld, D. Podolsky, and O. Cohen, Floquet group theory and its application to selection rules in harmonic generation, Nat. Commun. **10**, 405 (2019).
[113] M. Lysne, Y. Murakami, M. Schüler, and P. Werner, High-harmonic generation in spin-orbit coupled systems, Phys. Rev. B **102**, 081121(R) (2020).
[114] A. V. Kimel and M. Li, Writing magnetic memory with ultrashort light pulses, Nat. Rev. Mater. **4**, 189 (2019).
[115] Note that by increasing the duration of fsLPs, we have verified that noninteger HHG in Fig. 4 persists and thereby is not amenable to simplistic explanation from Ref. [96], where such harmonics for Hubbard ladders were related to the short duration of fsLPs, thus preventing the system from becoming fully time periodic.
[116] M. Ridley, L. Kantorovich, R. van Leeuwen, and R. Tuovinen, Quantum interference and the time-dependent radiation of nanojunctions, Phys. Rev. B **103**, 115439 (2021).
[117] O. D. Jefimenko, *Electricity and Magnetism* (Appleton-Century-Crofts, New York, 1966).
[118] D. J. Griffiths and M. A. Heald, Time-dependent generalizations of the Biot-Savart and Coulomb laws, Am. J. Phys. **59**, 111 (1991).
[119] K. T. McDonald, The relation between expressions for time-dependent electromagnetic fields given by Jefimenko and by Panofsky and Phillips, Am. J. Phys. **65**, 1074 (1997).

Correction: The omission of the value of t_{SO} below Eq. (5) has been fixed.

End Matter

To compute EM radiation generated by the charge dynamics, the expectation value $I_{ij} \equiv \langle \hat{I}_{ij} \rangle$ of the bond charge current operator [47],

$$\hat{I}_{ij} = \frac{ie}{\hbar} \sum_{\alpha} [\hat{\mathbf{c}}^{\dagger}_{i\alpha} \{ t_0(t)\hat{\sigma}_0 + \mathbf{t}_{\mathrm{SO}}(t) \} \hat{\mathbf{c}}_{j\alpha} - \mathrm{H.c.}], \quad \text{(A1)}$$

from site i to site j, with $\hat{\sigma}_0$ being a unit 2×2 matrix, is plugged into [34,93,116] the Jefimenko formula [117] for the electric field,

$$\mathbf{E}^{\mathrm{FF}}_{I}(\mathbf{r},t) = \frac{1}{4\pi\epsilon_0 c^2} \sum_{P_{i\to j}=1}^{N_b} \int_{P_{i\to j}} \left[(\mathbf{r}-\mathbf{l}) \frac{\partial_t I_{ij}(t_r)}{|\mathbf{r}-\mathbf{l}|^3} (\mathbf{r}-\mathbf{l}) \cdot \mathbf{e}_x - \frac{\partial_t I_{ij}(t_r)}{|\mathbf{r}-\mathbf{l}|} \mathbf{e}_x \right] dl. \quad \text{(A2)}$$

The most general Jefimenko formula [117], as the proper solution of the Maxwell equations [118], is reorganized [119] above to isolate the FF contributions decaying as $\sim 1/r$. Note that the Jefimenko equation (A2) can also be viewed [118] as the proper (i.e., time-retarded) time-dependent generalizations of the Coulomb law. Here $t_r \equiv t - |\mathbf{r}-\mathbf{l}|/c$ emphasizes retardation in the response time due to relativistic causality [117,119]. Additionally, we adapt [93,116] Eq. (A2) to utilize the expectation value of time-dependent bond charge currents [Eq. (A1)] as the source of EM radiation—they are the counterpart on the TB lattice of the local current density in continuous space. Such bond currents are assumed to be homogeneous [34,93,116] along the path $P_{i\to j}$ from site i to site j of length dl, N_b is the number of bonds, and we use the shorthand notation $\partial_t \equiv \partial/\partial_t$. Finally, we also compute the magnetic dipole contribution to FF radiation, as generated by the time dependence of the nonequilibrium magnetization,

$$\mathbf{E}^{\mathrm{FF}}_{M}(\mathbf{r},t) = \frac{1}{4\pi\epsilon_0 c^3} \sum_i \frac{\mathbf{r}-\mathbf{l}_i}{|\mathbf{r}-\mathbf{l}_i|^2} \times \partial_t^2 \mathbf{M}_i(t_r), \quad \text{(A3)}$$

where $\mathbf{l}_i$ indicates the location of the site i. Both contributions to EM radiation are computed at point P in Fig. 2, which is $100a_0$ away from NiO.

Supplemental Material for "Terahertz and High-Harmonic Radiation from Ultrafast Light Subgap or Above-Gap Driving of Spin-Orbit Proximitized Antiferromagnetic Mott Insulator"

Federico Garcia-Gaitan,[1] Adrian E. Feiguin,[2] and Branislav K. Nikolić[1,*]

[1] *Department of Physics and Astronomy, University of Delaware, Newark DE 19716, USA*
[2] *Department of Physics, Northeastern University, Boston, MA 02115, USA*

This Supplemental Material provides one additional Fig. S1 examining the efficiency of electron-spin interaction as a dissipation channel, where energy is transferred from the electrons to the spins. This channel is opened by our quasi-one-dimensional ladder geometry [1] (even faster relaxation by the same channel occurs in two-dimensional geometry [2]), as well as the presence of more than one orbital per its site [3]. That is, in dimensions greater than one, where spin-charge separation [4] characterizing 1D Mott insulators [4] is suppressed, an electron moving through an antiferromagnetically (AFM) ordered background flips a spin in every hopping process [2]. This process then leads to an intrinsically strong spin-charge interaction, that can be relevant even in the paramagnetic phase where spin correlations are short-ranged and short-lived [1].

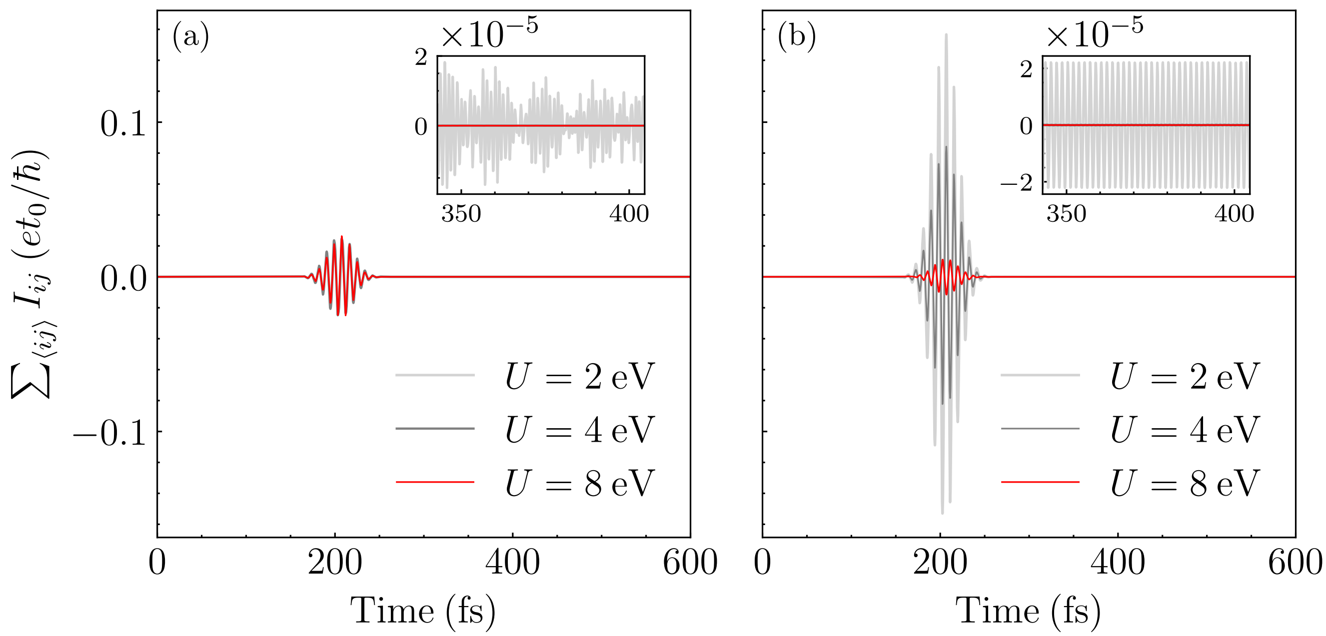

FIG. S1. Time dependence of the sum (over all pairs of nearest-neighbor sites, as denoted by $\langle ij\rangle$) of all bond charge currents [i.e., expectation values of bond current operator in Eq. (A1) of the main text] for: (a) fsLP-driven 2HHH model of NiO [Eq. (1) in the main text, but without proximity spin-orbit coupling term, $\hat{H}_{\rm SOC} = 0$], using different values of Hubbard U at fixed Hund coupling $J_H = 1$ eV; and (b) fsLP-driven plain Hubbard model with a single orbital per site on an identical ladder geometry. The central frequency of fsLP is subgap when compared to the Mott gap (Fig. 2 in the main text) opened by $U = 8$ eV.

Figure S1(a) confirms that the sum of all bond charge currents $\sum_{\langle ij\rangle} I_{ij}$ decays with increasing on-site Coulomb interaction (determined by Hubbard U). This is because as U increases, the system undergoes a phase transition from a metallic phase to a Mott insulating phase (note that we use $U = 8$ eV in the main text) favoring magnetic ordering, thereby enabling *dissipation of electron energy into bosonic excitations of AFM ordered background* [1, 2, 5]. Such current relaxation occurs despite the *absence* of phonons (as the other possible source of bosonic bath [6], but dissipating electron energy over much longer time scales [7]) in our calculations. We note that phonons are

* bnikolic@udel.edu

considered necessary [7] to relax femtosecond laser pulse (fsLP)-driven weakly correlated magnets and bring their charge photocurrents to zero [6]. Thus, we conclude that short-range spin correlations act as an efficient dissipative environment for mobile charge carriers in our two-orbital Hubbard-Hund-Heisenberg (2HHH) model [2, 5] of NiO. To understand the effect of its many orbitals per site, we also provide in Fig. S1(b) the result of the same calculations for the plain Hubbard model with a single orbital per site. By comparing Fig. S1(a) with Fig. S1(b) we learn that electron-spin dissipation channel associated with Hund coupling J_H (i.e., many orbitals per site) dominates at early times. On the other hand, the Hubbard U mediated dissipation mechanism becomes more relevant at longer times—this is clarified by the insets of both panels in Fig. S1 where current oscillations are suppressed, noticeably at later times, as U is increasing.

---

[1] M. Eckstein and P. Werner, Ultra-fast photo-carrier relaxation in Mott insulators with short-range spin correlations, Sci. Rep. **6**, 21235 (2016).

[2] D. Golež, J. Bonča, M. Mierzejewski, and L. Vidmar, Mechanism of ultrafast relaxation of a photo-carrier in antiferromagnetic spin background, Phys. Rev. B **89**, 165118 (2014).

[3] J. Rincón, E. Dagotto, and A. E. Feiguin, Photoinduced Hund excitons in the breakdown of a two-orbital Mott insulator, Phys. Rev. B **97**, 235104 (2018).

[4] Y. Murakami, S. Takayoshi, T. Kaneko, A. M. Läuchli, and P. Werner, Spin, charge, and η-spin separation in one-dimensional photodoped Mott insulators, Phys. Rev. Lett. **130**, 106501 (2023).

[5] K. Gillmeister, D. Golež, C.-T. Chiang, N. Bittner, Y. Pavlyukh, J. Berakdar, P. Werner, and W. Widdra, Ultrafast coupled charge and spin dynamics in strongly correlated NiO, Nat. Commun. **11**, 4095 (2020).

[6] A. Suresh and B. K. Nikolić, Quantum classical approach to spin and charge pumping and the ensuing radiation in terahertz spintronics: Example of the ultrafast light-driven Weyl antiferromagnet Mn_3Sn, Phys. Rev. B **107**, 174421 (2023).

[7] N. Wu, S. Zhang, D. Chen, Y. Wang, and S. Meng, Three-stage ultrafast demagnetization dynamics in a monolayer ferromagnet, Nat. Commun. **15**, 2804 (2024).